Environ Sci Pollut Res (2016) 23:15218–15226
DOI 10.1007/s11356-016-6702-5

RESEARCH ARTICLE

Core-shell Fe_3O_4@MIL-101(Fe) composites as heterogeneous catalysts of persulfate activation for the removal of Acid Orange 7

Xinxin Yue[1] · Weilin Guo[1] · Xianghui Li[1] · Haihong Zhou[1] · Ruiqin Wang[1]

Received: 16 January 2016 / Accepted: 15 April 2016 / Published online: 20 April 2016

Abstract In this study, a novel core-shell Fe_3O_4@MIL-101 (MIL stands for Materials of Institute Lavoisier) composite was successfully synthesized by hydrothermal method and was fully characterized by X-ray diffraction, transmission electron microscopy, Fourier-transform infrared spectra, and X-ray photoelectron spectroscopy. The composite was introduced as a catalyst to generate powerful radicals from persulfate for the removal of Acid Orange 7 in an aqueous solution. Effects of the central metal ions of MIL-101, amino group content of MIL-101, and pH were evaluated in batch experiments. It was found that both hydroxyl and sulfate radicals were generated; importantly, sulfate radicals were speculated to serve as the dominant active species in the catalytic oxidation of Acid Orange 7. In addition, a possible mechanism was proposed. This study provides new physical insights for the rational design of advanced metal-organic frameworks (MOF)-based catalysts for improved environmental remediation.

Keywords Metal-organic frameworks · Fe_3O_4 · Advanced oxidation processes · Acid Orange 7 · Sulfate radicals

Introduction

Nowadays, increasing water pollution has become a serious issue confronted by human beings, which promotes increasing demand for clean water environment. Advanced oxidation processes (AOPs) such as heterogeneous Fenton processes have been the focus of attention in recent years due to their potential effectiveness in the degradation and mineralization of organic contaminants in an aqueous solution (Lunar et al. 2000; Rodriguez et al. 2012; Yan et al. 2011). Recently, an innovative treatment technology based on persulfate oxidation has been studied as an alternative to conventional hydroxyl radicals-based advanced oxidation processes both for wastewater treatment (Deng et al. 2013; Fang et al. 2013; Gu et al. 2013; Khan et al. 2014; Romero et al. 2010) and in situ chemical oxidation applications (Lemaire et al. 2013; Liao et al. 2014). The persulfate anion ($S_2O_8^{2-}$) is a strong oxidant ($E°=2.1$ V), which through activation forms an even stronger sulfate radicals ($SO_4^{-\bullet}$, $E°=2.6$ V) (Tsitonaki et al. 2010). The main methods used for $SO_4^{-\bullet}$ generation are heat, UV or ultrasound activation, transition metal activation, alkaline activation, and peroxide activation (Chen and Su 2012). Among those, the addition of transition metal ions appears to be an inexpensive and practical way of achieving persulfate activation, but the potential health hazards caused by the dissolved metal ions (such as Fe^{2+}, Ag^{+}, or Co^{2+}) in water render such a homogeneous system with limited use (Leng et al. 2013).

Owing to the relatively wide availability and specific structural, magnetic, and catalytic properties of Fe_3O_4 particles, they have been applied as a suitable heterogeneous catalyst for activating persulfate (Leng et al. 2013). Structure and morphology of Fe_3O_4 particles can be modified for enhancing catalytic activity. On the other hand, the catalytic performance of Fe_3O_4 particles can be enhanced by supporting it with activated carbon, polymer membrane, silica, or zeolite.

As a new kind of porous material, metal-organic frameworks (MOFs) are a class of crystalline materials having infinite network structures built with multitopic organic ligands and metal ions. They have attracted significant research

Responsible editor: Bingcai Pan

✉ Weilin Guo
chm_guowl@ujn.edu.cn

[1] School of Resources and Environment, University of Jinan, Jinan 250022, China

interest in recent years, not only for their fundamental scientific interest but also for many attractive applications in catalysis (Corma et al. 2010), selective adsorption and separation (Li et al. 2009), gas storage (Zhao et al. 2011), and drug delivery (Horcajada et al. 2010; Horcajada et al. 2008; Taylor-Pashow et al. 2009). The use of MOFs as heterogeneous catalysts or supports for oxidations has been explored utilizing hydroperoxides or molecular oxygen as oxidants (Dhakshinamoorthy et al. 2011). Moreover, MOFs have an outstanding adsorption ability for some specific targets due to the "molecular sieving effect" and affinity interactions (Li et al. 2009).

Among the tens of thousands of known MOFs, the MIL (Materials of Institute Lavoisier) family built from trivalent metal centers and carboxylate bridging ligands pioneered by Férey and co-workers has particularly attracted a great deal of attention due to their enhanced stability, enormous porosity, and very large pores (Férey et al. 2005). MIL-53(Fe) was used to activate H_2O_2 for decomposing methylene blue dye with the help of visible light (Du et al. 2011). However, pure MIL catalysts possess only Fe(III) sites with weak Fenton activity and contain low iron-containing active sites. Therefore, a novel Fe(II)@MIL-100(Fe) heterogeneous catalyst was fabricated to enhance the catalytic performance by synergic effect between Fe(II) and Fe(III) active sites (Lv et al. 2015).

Recently, core-shell structured nanomaterials with a thin porous MOF shell have received much attention because of their intriguing properties that render them promising candidates for catalytic applications (Dhakshinamoorthy et al. 2011). The high surface area, diverse structural topologies, adjustable pore size, and tunable chemical properties of MOF shell, together with the functionality of nanoparticles cores such as magnetic, optical, and catalytic properties, can be effectively integrated. Until now, nanoparticles@MOFs such as have been successfully achieved and show potential applications in catalysis, drug delivery, gas storage, and gas separation (Taylor-Pashow et al. 2009; Zeng et al. 2015; Zhang et al. 2013a, b; Zhang et al. 2014). To the best of our knowledge, there is no previous report on the fabrication of core-shell Fe_3O_4@MIL composites as efficient catalysts to accommodate sulfate radical-based AOPs. MIL has a high surface area and when coated onto the surface of catalyst, it is able to enhance pollutant removal and degradation through synergistic adsorption-catalysis processes.

Herein, we report a facile route for synthesizing Fe_3O_4 nanoparticles on MIL-101(Fe) support to get Fe_3O_4@MIL-101(Fe) composites. Fe_3O_4@MIL-101(Fe) was characterized by X-ray diffraction (XRD), transmission electron microscope (TEM), X-ray photoelectron spectroscopy (XPS), and Fourier-transform infrared (FTIR) spectra. Acid Orange 7 (AO7), a kind of commonly used azo dyes, was selected to evaluate the catalytic activities due to its presence in the wastewater of several industries. Furthermore, some typical scavengers were added to identify the active species in the oxidation process, and the possible synergistic catalytic mechanism was proposed.

Experimental

Chemicals and reagents

Hydrated iron chloride ($FeCl_3 \cdot 6H_2O$), sodium acetate trihydrate ($NaAc \cdot 3H_2O$), ethylene glycol (EG), polyvinyl pyrrolidone (PVP), N, N-dimethylformamide (DMF), terephthalic acid (H_2BDC), ethanol, tert-butyl alcohol (TBA), and methanol (MeOH) were purchased from Aladdin Reagent Co. Ltd., China. Sodium hydroxide (NaOH), hydrochloric acid (HCl), 2-aminoterephthalic acid ($H_2BDC\text{-}NH_2$), aluminum chloride hexahydrate ($AlCl_3 \cdot 6H_2O$), chromic nitrate ($Cr(NO_3)_3 \cdot 9H_2O$), Acid Orange 7, and potassium persulfate ($K_2S_2O_8$) was obtained from Sinopharm Chemical Reagent Co. Ltd., China. All the chemical reagents were of analytical grade and used without further purification. Deionized water obtained from a Millipore Milli-Q system was used throughout the study.

Catalyst preparation and characterization

Fe_3O_4 nanoparticles were obtained by polyol process in a solvothermal system (Yan et al. 2007). In a typical procedure, $FeCl_3 \cdot 6H_2O$ (1.0 mmol) and $NaAc \cdot 3H_2O$ (5.0 mmol) were added to ethylene glycol (8.0 ml) to form a colloidal mixture under vigorous stirring at room temperature. Then, the mixture was sealed in a Teflon-lined stainless steel autoclave. Finally, the autoclave was heated and maintained at 160–180 °C for 10 h and then allowed to cool down to room temperature naturally. The back products were washed several times with deionized water.

For the Fe_3O_4@MIL-101(Fe) composite preparation, the freshly wet magnetic Fe_3O_4 particles (equal to 50 mg of dried Fe_3O_4) were dispersed in 5 mL of PVP (25 mg) DMF solution with ultrasonication for 10 min and then in 10 mL of $FeCl_3 \cdot 6H_2O$ (58.37 mg) DMF solution with ultrasonication for 10 min and then in 10 mL of H_2BDC (17.81 mg) DMF solution for another 10 min ultrasonication. The mixture was transferred into a Teflon-lined stainless steel autoclave and was heated at 110 °C for 20 h. Thereafter, the brown solid was separated from the reaction medium with an external magnet, washed with hot ethanol three times to remove impurities, and dried overnight at 70 °C in a vacuum drier. For comparison, pure MIL-101(Fe) powders were prepared by using current method in the absence of Fe_3O_4 particles (Zhang et al. 2014).

The crystalline structures of Fe_3O_4, MIL-101(Fe), and Fe_3O_4@MIL-101(Fe) were identified by a D/max-IIICX-ray diffractometer (Shimadzu, Japan). Fourier-transform infrared

spectra were taken with a Spectrum One FTIR spectrophotometer (Perkin-Elmer, USA) at room temperature. The X-ray photoelectron spectroscopy was carried out on a Kratos ASIS-HS X-ray photoelectron spectroscope fitted with a standard and monochromatic source (Al Kα) operated at 150 W (15 kV, 10 mA). Transmission electron microscopy (Tecnai G2 F20, FEI) was used to determine the shape and size distribution of the Fe_3O_4@MIL-101(Fe) composites.

Experimental procedure

All experiments were conducted in 50-mL beaker flasks under continuous magnetic stirring at pH of 3.58 unless specified elsewhere at room temperature.

The reaction was initiated immediately by adding 5 mL of 50 mmol L^{-1} persulfate and 0.01 g Fe_3O_4@MIL-101(Fe) to 5 mL of 50 mg L^{-1} AO7 solution. The pH values of the sample solutions were adjusted as required by using a pH meter, with small volumes of 0.01 mol L^{-1} HCl and NaOH. At given intervals, 5 mL of the suspension was extracted from each flask and subsequently centrifuged at 8000 rpm for 1 min with a TGL-16C centrifugal (Shanghai, China) to eliminate the sample powders. The concentrations of the residual AO7 were determined by monitoring decrease in absorbance at the maximum wavelength (484 nm) by UV-vis spectroscopy. Each degradation test was run in triplicate, and the averaged experimental values were then used.

For the recycle runs of AO7 degradation, the used catalyst was collected by centrifugation, washed with deionized water and ethanol, and dried in vacuum oven at 50 °C for 12 h. Owing to the small particle size, catalyst loss was unavoidable in the process of washing and drying. Thus, several parallel reactions were conducted in the three runs to ensure that the dose of recycled catalyst was sufficient for the next run. Catalyst dose and other reaction conditions remained the same for the subsequent runs.

Results and discussion

Synthesis and structure characterization of core-shell Fe_3O_4@MIL-101(Fe) composites

Powder X-ray diffraction patterns of Fe_3O_4, MIL-101(Fe), and Fe_3O_4@MIL-101(Fe) core-shell composite are shown in Fig. 1a. The peaks at 2θ of 30.5°, 35.7°, 43.3°, 57.8°, and 63.0°, corresponding to (220), (311), (400), (511), and (440) reflections of the cubic spinel structure, matched well with the characteristic peaks of Fe_3O_4 (JCPDS No. 19-0629). The powder XRD pattern of MIL-101(Fe) was also in accordance with the literature (Skobelev et al. 2013). Five characteristic peaks for Fe_3O_4 and two characteristic peaks for MIL-101(Fe) were preserved in the graph of the Fe_3O_4@MIL-101(Fe) composite, revealing that this hybrid material was composed of Fe_3O_4 and MIL-101(Fe).

The surface property of Fe_3O_4, MIL-101(Fe), and Fe_3O_4@MIL-101(Fe) was monitored by FTIR spectra (Fig. 1b). In the spectrum of Fe_3O_4, the broad peaks centered at 3400 and 1600 cm^{-1} were attributed to the stretching vibrations of adsorbed water and hydroxyl groups. The prominent peaks at 580 and 403 cm^{-1} were ascribed to the intrinsic Fe–O stretching modes of the tetrahedral and octahedral sites, respectively. For MIL-101, the peak at 741 cm^{-1} was attributed to the out-of-plane bending vibration of C–H in the benzene ring of H_2BDC (Zhang et al. 2013a, b). The bands at 1681 and 1506 cm^{-1} were assigned to the asymmetric stretching of carboxyl groups, whereas the band at 1385 cm^{-1} was assigned to the symmetric stretching of carboxyl groups in H_2BDC. The spectrum of Fe_3O_4@MIL-101(Fe) showed adsorption at 580 cm^{-1}, confirming the existence of Fe_3O_4.

As can be seen from TEM image shown in Fig. 1c, the finally formed Fe_3O_4@MIL-101(Fe) composites were composed of a Fe_3O_4 core and a MIL-101(Fe) shell, clearly demonstrating the formation of a core-shell structure. It shows that the average diameter of the Fe_3O_4@MIL-101(Fe) nanoparticles was approximately 100 nm and the MIL-101(Fe) shell was about 12.5 nm.

The existence of Fe_3O_4 was further confirmed by X-ray photoelectron spectroscopy. As shown in Fig. 1d, elemental C, O, and Fe existed in the Fe_3O_4@MIL-101(Fe) composites. The peaks located at about 711.3 and 722.7 eV represented the binding energies of Fe 2p3/2 and Fe 2p1/2, respectively, and the Fe 2p3/2 peak can be split into two peaks at 710.3 and 713.0 eV, which indicate the presence of Fe(II) and Fe(III), consistent with the literature data for Fe_3O_4 (Xu and Wang 2012). And the XPS spectrum varied little before and after reaction, which indicates that Fe_3O_4@MIL-101(Fe) is stable.

Catalytic performance of Fe_3O_4@MIL-101(Fe)

To evaluate the degradation efficiency of AO7 under different systems, the following experiments were conducted: Fe_3O_4 alone, persulfate alone, MIL-101(Fe) alone, Fe_3O_4@MIL-101(Fe) alone, Fe_3O_4/persulfate process, MIL-101(Fe)/persulfate process, and Fe_3O_4@MIL-101(Fe)/persulfate process. The results are shown in Fig. 2. It can be obviously seen that no appreciable AO7 removal was observed when adding into the AO7 solution with Fe_3O_4 alone, indicating the effect of adsorption on AO7 removal was not obvious under the condition investigated. Little removal also occurred when persulfate alone was applied. Persulfate is stable at ambient temperature, and its oxidation power was limited ($E°$ = 2.01 V) (Wu et al. 2012; Zhao et al. 2010), which could hardly degrade AO7. When treated over Fe_3O4@MIL-101(Fe) or MIL-101(Fe) alone, 33.4 and 56.8 % of 25 mg L^{-1} AO7 was decolorized, respectively. The removal of AO7 by MIL-101(Fe)

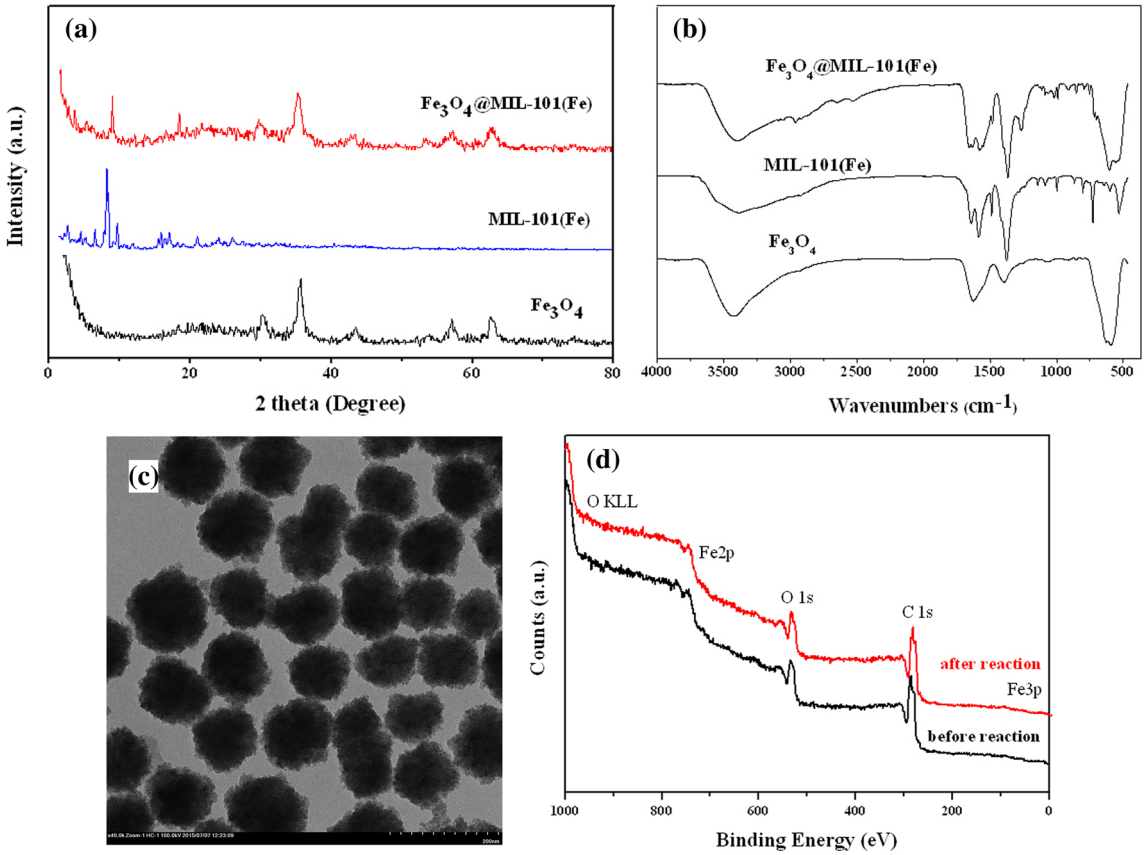

Fig. 1 **a** XRD patterns and **b** FTIR spectra of Fe_3O_4, MIL-101(Fe), and Fe_3O_4@MIL-101(Fe). **c** TEM micrograph of Fe_3O_4@MIL-101(Fe) and **d** XPS wide-scan survey of Fe_3O_4@MIL-101(Fe) before and after reaction

was higher than by Fe_3O_4@MIL-101(Fe) obviously, it is because that MIL-101(Fe) has larger specific surface area and pore size; as a result, MIL-101(Fe) has better adsorption of AO7 compared with Fe_3O_4@MIL-101(Fe) in the same quality. In the presence of persulfate, AO7 removal achieved to, respectively, 53.6, 65.5, and 98.1 % for Fe_3O_4, MIL-101(Fe), and Fe_3O_4@MIL-101(Fe) after 60 min, which was due to the synergistic effect between Fe_3O_4 and MIL-101(Fe). The results indicate that Fe_3O_4@MIL-101(Fe) composites exhibit enhanced catalytic activities for the removal of AO7 as compared with pure materials under the same condition. On the one hand, Fe3O4@MIL-101(Fe) can absorb much more AO7 on composite surface due to the presence of MIL-101(Fe). On the other hand, the Fe(II) species formed on the catalyst surface can effectively activate persulfate to generate radicals via Eq. 1 [Liang et al. 2004]. In addition, hydroxyl radicals can also be formed via the following reactions (Eqs. 2 and 3) and may participate in contaminant oxidation.

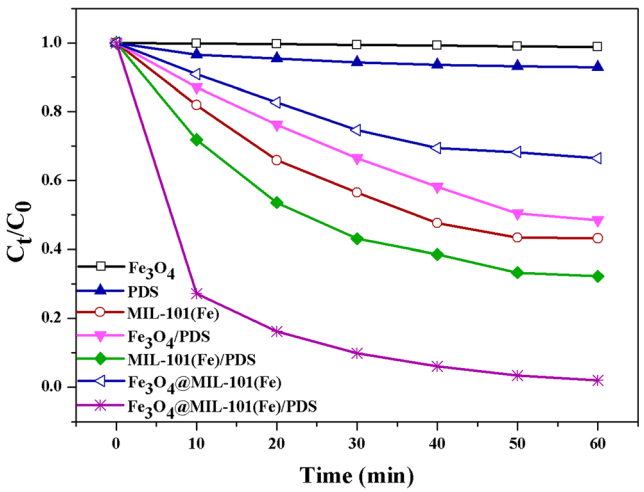

Fig. 2 Removal of AO7 under different processes (AO7, 25 mg L^{-1}; persulfate, 25 mmol L^{-1}; catalyst, 1.0 g L^{-1}; pH, 3.58)

$$\mathrm{Fe(II)} + \mathrm{S_2O_8^{2-}} \rightarrow \mathrm{SO_4^{-\bullet}} + \mathrm{SO_4^{2-}} + \mathrm{Fe(III)} \quad (1)$$

$$\text{All pH:}\ \mathrm{SO_4^{-\bullet}} + \mathrm{H_2O} \rightarrow \mathrm{H^+} + \mathrm{SO_4^{2-}} + {}^{\bullet}\mathrm{OH} \quad (2)$$

$$\text{Alkaline pH:}\ \mathrm{SO_4^{-\bullet}} + \mathrm{OH^-} \rightarrow \mathrm{SO_4^{2-}} + {}^{\bullet}\mathrm{OH} \quad (3)$$

To quantitatively evaluate the synergistic effect, the synergistic factor f is proposed and calculated using the following formula:

$$f = \frac{k_{\mathrm{Fe_3O_4@MIL-101(Fe)}}}{k_{\mathrm{Fe_3O_4}} + k_{\mathrm{MIL-101(Fe)}}} \quad (4)$$

where $k_{Fe3O4@MIL-101(Fe)}$, k_{Fe3O4}, and $k_{MIL-101(Fe)}$ are the fitted reaction rate constants of Fe_3O_4@MIL-101(Fe), Fe_3O_4, and MIL-101(Fe), respectively. The synergistic factor is 2.12, which is bigger than 1.0, suggesting there exists positive interactions between pure materials for enhancing catalytic activities.

Analogous MOFs composed of different metal ions with similar MOF structures, such as MIL-101(Al), MIL-101(Cr), and MIL-101(Fe), were also compared to understand any effects of the central metal ions on the removal of AO7. Figure 3 shows the removal results of AO7 over Fe_3O_4@MIL-101(M) (M = Fe, Cr, Al). It can be seen that the central ions of MIL-101 could influence the removal of AO7 and Fe_3O_4@MIL-101(Fe) catalyst exhibited highest Fenton oxidation catalytic ability. Besides the surface iron active sites in Fe_3O_4, iron ions on the surface of MIL-101(Fe) can effectively catalyze the decomposition of persulfate to produce sulfate radicals. While for Fe_3O_4@MIL-101(Cr) and Fe_3O_4@MIL-101(Al), low catalytic activity was observed and the decolorization efficiencies of AO7 were about 80.3 and 88.7 % after 60 min, respectively. The catalytic degradation performances of Fe_3O_4@MIL-100 species for AO7 are on the order of Fe_3O_4@MIL-101(Fe) > Fe_3O_4@MIL-101(Cr) > Fe_3O_4@MIL-101(Al). Therefore, the central metal ions of MOFs play a significant role in the catalytic removal of AO7.

In order to investigate the influence of functional groups in the linkers of MOFs on the degradation of AO7, a series of Fe_3O_4@MIL-101(Fe)–NH_2 composites with different incorporated amino group content was directly prepared by using a mixed linker strategy that combined H_2BDC with H_2BDC–NH_2 during the synthesis. It can be seen from Fig. 4 that the amino group in the linker of MOFs strongly influenced the degradation of AO7, and the degradation efficiency decreased with increasing the amount of amino group. The results are ascribed to the repulsive interaction between the amino group and AO7 molecules. The AO7 molecules exhibit the aqueous

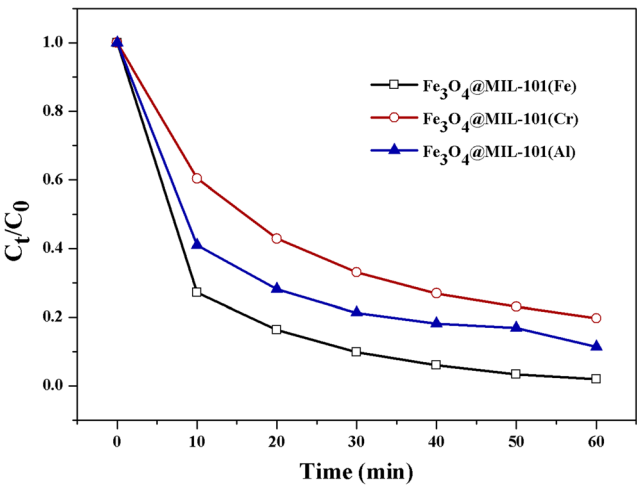

Fig. 3 Effect of central metal atom of Fe_3O_4@MIL-101(M) (M = Fe, Cr, Al) on the removal of AO7 (AO7, 25 mg L^{-1}; persulfate, 25 mmol L^{-1}; catalyst, 1.0 g L^{-1}; pH, 3.58)

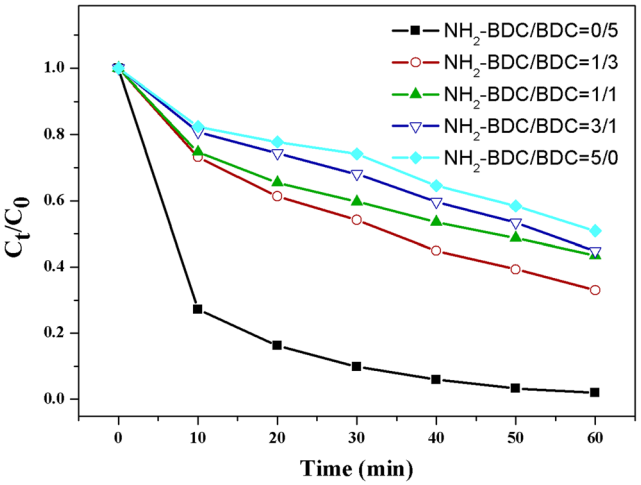

Fig. 4 Effect of amino group content in MIL-101(Fe) on the removal of AO7 (AO7, 25 mg L^{-1}; persulfate, 25 mmol L^{-1}; catalyst, 1.0 g L^{-1}; pH, 3.58)

dissociation constants as pKa = 11.4, as a result, AO7 is positively charged in most of the experimental pH range (about 3.58). On the other hand, we measured the zeta potential of the Fe_3O_4@MIL-101(Fe)–NH_2 composites and found that the surface of the catalyst charge remained positive below a pH of 8.1 and became negative at higher pH values (>8.1). Thus, the adsorption capacity of the catalysts decreased gradually with increasing the amount of amino group, which was probably due to the electrostatic repulsion of positively charged catalysts and positive AO7 molecules.

The pH value of the reaction solution is usually a crucial parameter affecting the oxidative degradation of organic pollutants. Therefore, the effect of pH was investigated by varying the pH from 1.86 to 11.62. All of the experiments were conducted at 25 °C, 25.0 mmol L^{-1} $K_2S_2O_8$, 1.0 g L^{-1} Fe_3O_4@MIL-101(Fe), and 25 mg L^{-1} AO7. As can be shown in Fig. 5, the highest rate of AO7 removal was generated at

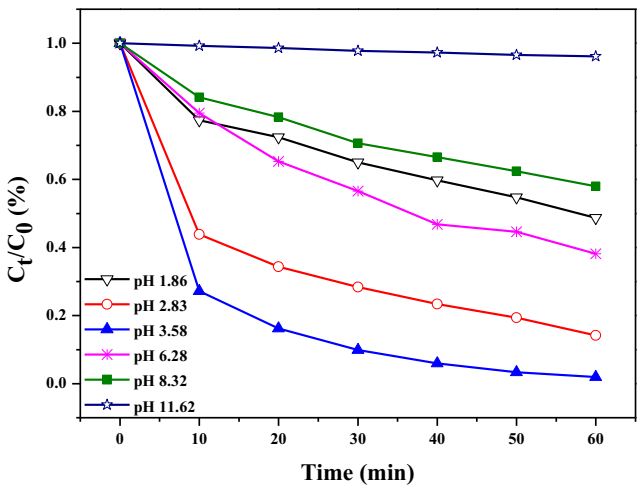

Fig. 5 Effect of the initial pH on the removal of AO7 (AO7, 25 mg L^{-1}; persulfate, 25 mmol L^{-1}; catalyst, 1.0 g L^{-1}; pH, 3.58)

pH 3.58. When the initial pH increased from 1.86 to 3.58, the removal rate quickly increased, and it decreased when the pH was raised from 3.58 to 11.62. A reason for this phenomenon might be that the acid condition may favor the dissolution of Fe, and a higher amount of Fe^{2+} was produced under the acidic condition, in which $SO_4^{-\bullet}$ is generated more rapidly to degrade AO7 compared with any other conditions. However, at pH < 3.58, the regeneration of Fe^{2+} (Eq. 5) could be limited which causes a reduced generation of $SO_4^{-\bullet}$ and hence lower mineralization of AO7 (Lin and Gurol 1998). When the initial pH increased from 3.58 to 11.62, the removal rate of AO7 decreased remarkably, which might be due to the rapid decay of $SO_4^{-\bullet}$ resulting from the reactions with water or hydroxyl ions (Eqs. 2 and 3) (Wu 2008).

$$Fe^{3+} + H_2O \rightarrow FeOH^{2+} + H^+ \quad (5)$$

Possible mechanism

To better understand the role of Fe species in the activation of persulfate, XPS spectra of fresh and used catalysts were recorded and the results are shown in Fig. 6. All Fe 2p spectra showed two main peaks at binding energies of 711.3 and 722.7 eV, which are assigned to Fe 2p3/2 and Fe 2p1/2, respectively. The high-resolution spectra of the peaks at 710.3 and 713.0 eV are indicative of the presence of Fe(II) and Fe(III). After the reaction, the binding energies slightly shifted and the area of Fe(II) at 710.3 eV decreased from 64.2 to 54.8 %, indicating the oxidation of Fe(II) into Fe(III) species. This is probably attributed to the reaction between Fe(II) and persulfate.

As shown in Fig. 7, the typical electrochemical impedance spectra were presented as Nyquist plots, and it is observed that Fe_3O_4@MIL-101(Fe) had lower resistance than that of pure Fe_3O_4 and MIL-101(Fe), which indicated a decrease in the solid state interface layer resistance and the charge transfer

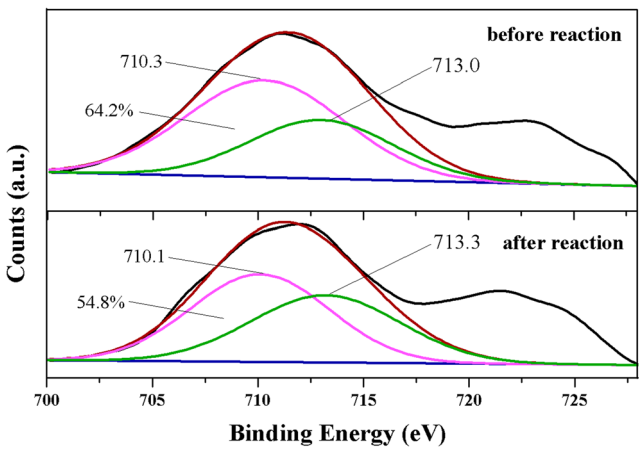

Fig. 6 XPS spectra for Fe 2p regions of Fe_3O_4@MIL-101(Fe) before and after reaction

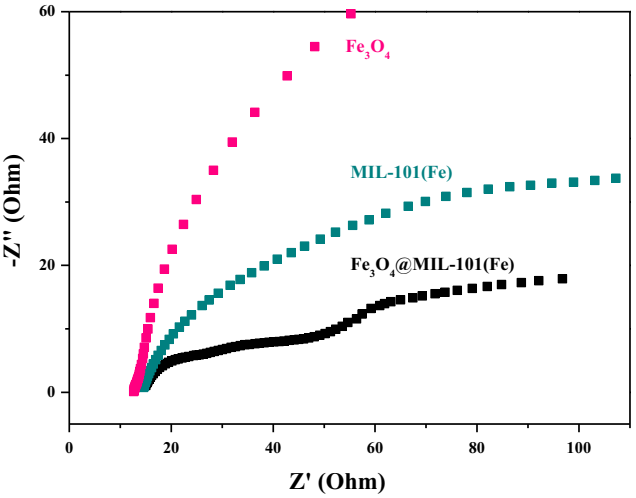

Fig. 7 Electrochemical impedance spectroscopy of Fe_3O_4, MIL-101(Fe), and Fe_3O_4@MIL-101(Fe)

resistance on the surface (Zhu et al. 2007). This means there existed certain synergistic interaction between MIL-101(Fe) and Fe_3O_4. Therefore, the strong interaction played an important role in enhancing the catalytic activity of the composites, which was attributed to the electron transfer between iron active sites of Fe_3O_4 and iron active sites of MIL-101(Fe), resulting in the effective redox cycling of iron between Fe(II) and Fe(III).

It is well reported that a series of reactive oxygen species, such as $SO_4^{-\bullet}$, $^{\bullet}OH$, and $O_2^{-\bullet}$, were generated in a Fe-activated persulfate system. To verify the radical type present in the Fe_3O_4@MIL-101(Fe)-activated persulfate process, a few quenching tests were carried out by using methanol (MeOH), tert-butyl alcohol (TBA), and 1, 4-benzoquinone (BQ) (Su et al. 2013). Methanol ensures the quenching of both $SO_4^{-\bullet}$ (3.2×10^6 $M^{-1}s^{-1}$) and $^{\bullet}OH$ (9.7×10^8 $M^{-1}s^{-1}$) owing to the high reactivity toward the two radicals, whereas TBA mainly reacts with $^{\bullet}OH$ (6.0×10^8 $M^{-1}s^{-1}$) and is not effective for $SO_4^{-\bullet}$ (8.0×10^5 $M^{-1}s^{-1}$). As shown in Fig. 8, when no quenching agent was added, about 98.1 % AO7 was degraded in 60 min. However, the addition of 1.0 mol L^{-1} methanol nearly entirely inhibited the removal of AO7, which meant that the radicals generated in the system were mostly quenched. Meanwhile, the removal efficiency of AO7 was decreased from 98.1 to 67.2 % in 60 min with the addition of 1.0 mol L^{-1} TBA, meaning that $^{\bullet}OH$ has little contribution on the AO7 decomposition. To investigate the role of $O_2^{-\bullet}$, BQ is used as $O_2^{-\bullet}$ (9.6×10^8 $M^{-1}s^{-1}$) quencher in this study. The addition of 1.0 mol L^{-1} BQ resulted in decreasing AO7 removal to 73.8 % after 60 min, which indicate that $O_2^{-\bullet}$ radicals were involved in the oxidation process. All of these results confirmed the involvement of $SO_4^{-\bullet}$, $^{\bullet}OH$, and $O_2^{-\bullet}$ radicals in the Fe_3O_4@MIL-101(Fe)/persulfate oxidation process, and $SO_4^{-\bullet}$ is the predominant reactive oxygen species responsible for the AO7 removal, which agrees with recent

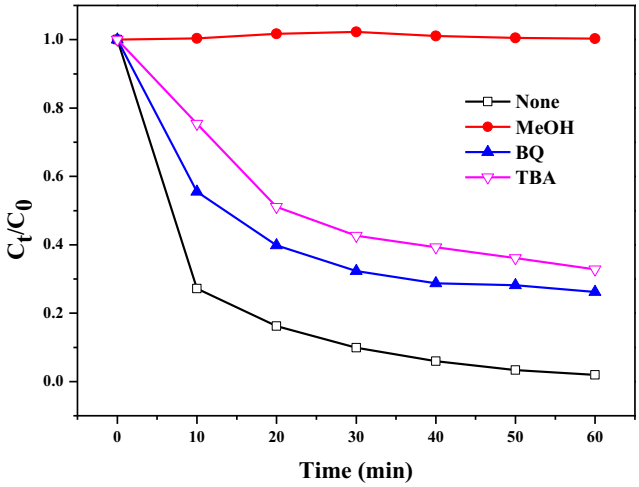

Fig. 8 Effect of radical scavengers on the removal of AO7 (AO7, 25 mg L^{-1}; persulfate, 25 mmol L^{-1}; catalyst, 1.0 g L^{-1}; pH, 3.58)

findings in the literature (Ding et al. 2013; Khan et al. 2013; Yao et al. 2015; Zhang et al. 2013a, b).

Based on the results above, main processes during the catalytic activation of persulfate by Fe_3O_4@MIL-101(Fe) are proposed as follows (Fig. 9).

Magnetite is one of the most stable mixed-valence oxides (Fe(II)–Fe(III)) at ambient temperature. Fe(II) species on the catalyst surface can effectively react with persulfate to produce sulfate radicals, and then, more Fe(II) species are regenerated by the reactions between the formed Fe(III) species and persulfate. On the one hand, the metal ions or metal clusters of MOFs not only play a role in maintaining the structure but also have the potential of catalytic activity. Fe(II) was generated by the reduction and transformation of Fe(III) on the surface of MIL-101(Fe) structure and then activated persulfate to release sulfate radicals (Lv et al. 2015). On the other hand, the synergistic interaction between MIL-101(Fe) and Fe_3O_4 favored the in situ recycling of Fe(II) and Fe(III) sites in catalyst. Meanwhile, hydroxyl radicals were generated by the reaction between sulfate radicals and H_2O or OH^-. Moreover, MIL-101(Fe) has large specific surface area and high porosity, which favors the adsorption of contaminants, resulting in more efficient degradation of pollutants (Zeng et al. 2015).

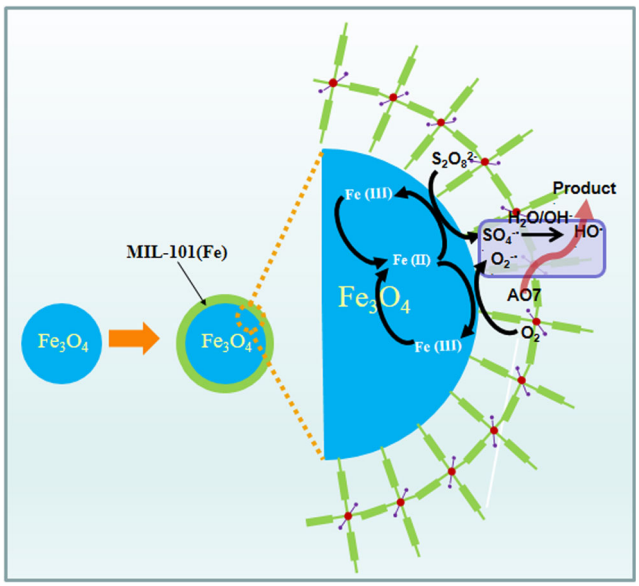

Fig. 9 Proposed mechanism of AO7 in the Fe_3O_4@MIL-101(Fe)/persulfate system

Cycling tests

In order to check the recycling efficiency of the catalyst, the cycling tests were conducted. The catalyst could be easily and rapidly separated from the reaction mixture. The initial concentration of AO7 solution was fixed at 25 mg L^{-1}, persulfate concentration was 25 mmol L^{-1}, Fe_3O_4@MIL-101(Fe) was 1.0 g L^{-1}, and the initial pH was 3.58. As shown in Fig. 10, the removal efficiencies of AO7 during three reaction cycles ranged from 98.1 to 95.0 %. Moreover, inductively coupled plasma-atomic emission spectrometric (ICP-AES) analysis indicated that the Fe^{3+} leaching was less than 15 μg L^{-1} under the tested reaction conditions. So, the above findings indicate that the Fe_3O_4@MIL-101(Fe) composites have high stability and good reusability.

Conclusions

Aqueous solutions of AO7 have been degraded effectively in the Fe_3O_4@MIL-101(Fe)/persulfate process, in which Fe_3O_4-activated persulfate process is enhanced by the metal organic framework. The effect of initial pH, amino group content in the linker of MIL-101, central metal ions of MIL-101, and the

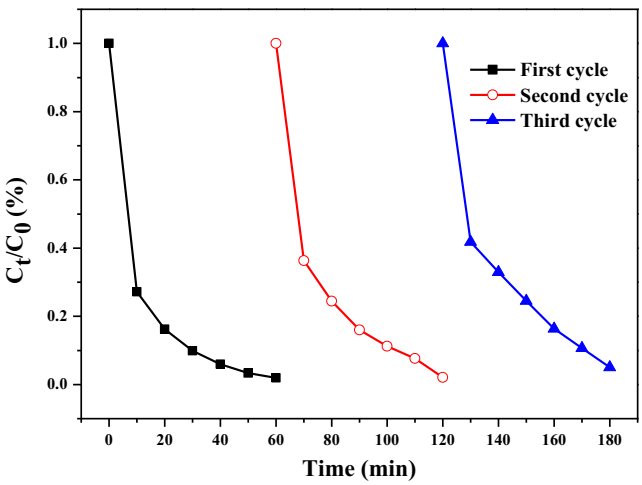

Fig. 10 Degradation performance of recycled catalyst (AO7, 25 mg L^{-1}; persulfate, 25 mmol L^{-1}; catalyst, 1.0 g L^{-1}; pH, 3.58)

radical scavengers on the AO7 removal was investigated. The results indicated that AO7 can be totally degraded in a 60-min reaction when initial AO7 concentration was 25 mg L^{-1}, persulfate concentration was 25 mmol L^{-1}, Fe_3O_4@MIL-101(Fe) was 1.0 g L^{-1}, and initial pH was 3.58. It is clear that the AO7 removal efficiency over Fe_3O_4@MIL-101(Fe) was much higher than that of Fe_3O_4 and MIL-101(Fe). Recycle experiments showed the Fe_3O_4@MIL-101(Fe) composites were stable and can be reused. Thus, the Fe_3O_4@MIL-101(Fe)/persulfate process can be an effective technology for treating wastewater containing resistant organic compounds.

Acknowledgments This work was financially supported by the National Natural Science Foundation, China (Grant No. 51578264), the Shandong Provincial Natural Science Foundation, China (Grant No. ZR2013EEM004), and the Shandong Provincial Science and Technology Development Program, China (Grant No. 2014GSF117008).

References

Chen WS, Su YC (2012) Removal of dinitrotoluenes in wastewater by sonoactivated persulfate. Ultrason Sonochem 19:921–927

Corma A, García H, Llabrési FX (2010) Engineering metal organic frameworks for heterogeneous catalysis. Chem Rev 110:4606–4655

Deng J, Shao Y, Gao N, Deng Y, Zhou S, Hu X (2013) Thermally activated persulfate (TAP) oxidation of antiepileptic drug carbamazepine in water. Chem En J 228:765–771

Dhakshinamoorthy A, Alvaro M, Garcia H (2011) Metal-organic frameworks as heterogeneous catalysts for oxidation reactions. Catal Sci Technol 1:856–867

Ding Y, Zhu L, Wang N, Tang H (2013) Sulfate radicals induced degradation of tetrabromobisphenol A with nanoscaled magnetic $CuFe_2O_4$ as a heterogeneous catalyst of peroxymonosulfate. Appl Catal B Environ 129:153–162

Du JJ, Yuan YP, Sun JX, Peng FM, Jiang X, Qiu LG, Xie AJ, Shen YH, Zhu JF (2011) New photocatalysts based on MIL-53 metal-organic frameworks for the decolorization of methylene blue dye. J Hazard Mater 190:945–951

Fang GD, Dionysiou DD, Zhou DM, Wang Y, Zhu XD, Fan JX, Cang L, Wang YJ (2013) Transformation of polychlorinated biphenyls by persulfate atambient temperature. Chemosphere 90:1573–1580

Férey G, Mellot-Draznieks C, Serre C, Millange F (2005) Crystallized frameworks with giant pores: are there limits to the possible? Acc Chem Res 38:217–225

Gu X, Lu S, Qiu Z, Sui Q, Banks CJ, Imai T, Lin K, Luo Q (2013) Photodegradation performance of 1,1,1-trichloroethane in aqueous solution: in the presence and absence of persulfate. Chem Eng J 215–216:29–35

Horcajada P, Serre C, Maurin G, Ramashye NA, Balas F, Vallet-Regí M, Sebban M, Taulelle F, Férey G (2008) Flexible porous metal-organic frameworks for a controlled drug delivery. J Am Chem Soc 130: 6774–6780

Horcajada P, Chalati T, Serre C, Gillet B, Sebrie C, Baati T, Eubank JF, Heurtaux D, Clayette P, Kreuz C, Chang JS, Hwang YK, Marsaud V, Bories PN, Cynober L, Gil S, Férey G, Couvreur P, Gref R (2010) Porous metal-organic framework nanoscale carriers as a potential platform for drug delivery and imaging. Nat Mater 9:172–178

Khan JA, He X, Khan HM, Shah NS, Dionysiou DD (2013) Oxidative degradation of atrazine in aqueous solution by UV/H_2O_2/Fe^{2+}, UV/$S_2O_8^{2-}$/Fe^{2+} and UV/HSO_5^-/Fe^{2+} processes: a comparative study. Chem Eng J 218:376–383

Khan JA, He X, Shah NS, Khan HM, Hapeshi E, Fatta-Kassinos D, Dionysiou DD (2014) Kinetic and mechanism investigation on the photochemical degradation of atrazine with activated H_2O_2, $S_2O_8^{2-}$ and HSO_5^-. Chem Eng J 252:393–403

Lemaire J, Buès M, Kabeche T, Hanna K, Simonnot MO (2013) Oxidant selection to treat an aged PAH contaminated soil by in situ chemical oxidation. J Environ Chem Eng 1:1261–1268

Leng YQ, Guo WL, Shi X, Li YY, Xing LT (2013) Polyhydroquinone-coated Fe_3O_4 nanocatalyst for degradation of rhodamine B based on sulfate radicals. Ind Eng Chem Res 52:13607–13612

Li JR, Kuppler RJ, Zhou HC (2009) Selective gas adsorption and separation in metal-organic frameworks. Chem Soc Rev 38:1477–1504

Liang CJ, Bruell CJ, Marley MC, Sperry KL (2004) Persulfate oxidation for in situ remediation of TCE. I. Activated by ferrous ion with and without a persulfate-thiosulfate redox couple. Chemosphere 55: 1213–1223

Liao X, Zhao D, Yan X, Huling SG (2014) Identification of persulfate oxidation products of polycyclic aromatic hydrocarbon during remediation of contaminated soil. J Hazard Mater 276:26–34

Lin S, Gurol MD (1998) Catalytic decomposition of hydrogen peroxide on iron oxide: kinetics, mechanism, and implications. Environ Sci Technol 32:1417–1423

Lunar L, Sicilia D, Rubio S, Pearez-Bendito D, Nicke U (2000) Degradation of photographic developers by Fenton's reagent: condition optimization and kinetics for metal oxidation. Water Res 34: 1791–1802

Lv HL, Zhao HY, Cao TC, Qian L, Wang YB, Zhao GH (2015) Efficient degradation of high concentration azo-dye wastewater by heterogeneous Fenton process with iron-based metal-organic framework. J Mol Catal A Chem 400:81–89

Rodriguez S, Santos A, Romero A, Vicente F (2012) Kinetic of oxidation and mineralization of priority and emerging pollutants by activated persulfate. Chem Eng J 213:225–234

Romero A, Santos A, Vicente F, González C (2010) Diuron abatement using activated persulphate: effect of pH, Fe(II) and oxidant dosage. Chem Eng J 16:257–265

Skobelev IY, Sorokin AB, Kovalenko KA, Fedin VP, Kholdeeva OA (2013) Solvent-free allylic oxidation of alkenes with O_2 mediated by Fe- and Cr-MIL-101. J Catal 298:61–69

Su SN, Guo WL, Leng YQ, Yi CL, Ma ZM (2013) Heterogeneous activation of Oxone by $Co_xFe_{3-x}O_4$ nanocatalysts for degradation of Rhodamine B. J Hazard Mater 244–245:736–742

Taylor-Pashow KML, Rocca JD, Xie ZG, Tran S, Lin WB (2009) Postsynthetic modifications of iron-carboxylate nanoscale metal-organic frameworks for imaging and drug delivery. J Am Chem Soc 131:14261–14263

Tsitonaki A, Petri B, Crimi M, Mosbaek H, Siegrist RL, Bjerg PL (2010) In situ chemical oxidation of contaminated soil and groundwater using persulfate: a review. Crit Rev Environ Sci Technol 40:55–91

Wu CH (2008) Reactive Red 198 in UV/TiO_2-based systems. Dyes Pigments 71:31–38

Wu J, Zhang H, Qiu JJ (2012) Degradation of Acid Orange 7 in aqueous solution byanovel electro/Fe^{2+}/peroxydisulfate process. J Hazard Mater 215–216:138–145

Xu LJ, Wang JL (2012) Fenton-like degradation of 2,4-dichlorophenol using Fe_3O_4 magnetic nanoparticles. Appl Catal B Environ 123–124:117–126

Yan AG, Liu XH, Qiu GZ, Zhang N, Shi RR, Yi R, Tang MT, Che RC (2007) A simple solvothermal synthesis and characterization of round-biscuit-like Fe_3O_4 nanoparticles with adjustable sizes. Solid State Commun 144:315–318

Yan JC, Lei M, Zhu LH, Anjum MN, Zou J, Tang HQ (2011) Degradation of sulfamonomethoxine with Fe_3O_4 magnetic

nanoparticles as heterogeneous activator of persulfate. J Hazard Mater 186:1398–1404

Yao YJ, Cai YM, Wu GD, Wei FY, Li XY, Chen H, Wang SB (2015) Sulfate radicals induced from peroxymonosulfate by cobalt manganese oxides ($CoxMn_{3-x}O_4$) for Fenton-like reaction in water. J Hazard Mater 296:128–137

Zeng T, Zhang XL, Wang SH, Niu HY, Cai YQ (2015) Spatial confinement of Co_3O_4 catalyst in hollow metal-organic framework as nanoreactor for improved degradation of organic pollutant. Environ Sci Technol 49:2350–2357

Zhang SL, Du Z, Li GK (2013a) Metal-organic framework-199/graphite oxide hybrid composites coated solid-phase microextraction fibers coupled with gas chromatography for determination of organochlorine pesticides from complicated samples. Talanta 115:32–39

Zhang T, Zhu H, Croué JP (2013b) Production of sulfate radical from peroxymonosulfate induced by a magnetically separable $CuFe_2O_4$ spinel in water: efficiency, stability, and mechanism. Environ Sci Technol 47:2784–2791

Zhang SL, Jiao Z, Yao WX (2014) A simple solvothermal process for fabrication of a metal-organic framework with an iron oxide enclosure for the determination of organophosphorus pesticides in biological samples. J Chromatogr A 1371:74–81

Zhao JY, Zhang YB, Quan X, Chen S (2010) Enhanced oxidation of 4-chlorophenolusing sulfate radicals generated from zero-valent iron and peroxydisulfate at ambient temperature. Sep Purif Technol 71: 302–307

Zhao D, Timmons DJ, Yuan DQ, Zhou HC (2011) Tuning the topology and functionality of metal-organic frameworks by ligand design. Acc Chem Res 44:123–133

Zhu SB, Xu TG, Fu HB, Zhao JC, Zhu YF (2007) Synergetic effect of Bi_2WO_6 photocatalyst with C_{60} and enhanced photoactivity under visible irradiation. Environ Sci Technol 41:6234–6239